Structural Features of the C-Terminal Domain of Bovine Rhodopsin: A Site-Directed Spin-Labeling Study[†,‡]

Ralf Langen,[§] Kewen Cai,[||] Christian Altenbach,[§] H. Gobind Khorana,*[,||] and Wayne L. Hubbell*[,§]

Jules Stein Eye Institute and Department of Chemistry and Biochemistry, University of California, Los Angeles, California 90095, and Departments of Biology and Chemistry, Massachusetts Institute of Technology, Cambridge, Massachusetts 02139

Received January 4, 1999; Revised Manuscript Received April 8, 1999

ABSTRACT: Eleven single-cysteine substitution mutants have been prepared in the sequence 325−340 of rhodopsin, corresponding to the C-terminal domain. Each of the cysteine mutants was modified with a selective nitroxide reagent to introduce a spin-labeled side chain. The electron paramagnetic resonance spectra of the labeled proteins were analyzed in terms of side chain dynamics. At all sites, the spectra reflected the presence of two populations of different mobility, although one was always dominant. The mobility of the dominant population increased in a regular fashion from the palmitoylation sites at 322C and 323C to the C-terminus, where the spectra resembled those of an unfolded protein. This apparent mobility gradient is only slightly affected in mutants lacking the palmitoyl groups, suggesting that they are not responsible for physically anchoring the C-terminal peptide at one end. Binding of a monoclonal antibody to its epitope at the C-terminus dramatically reduces the mobility of nearby residues, creating a local mobility gradient opposite that in the absence of the antibody. These results indicate that the C-terminal domain of rhodopsin, beyond the palmitoylation sites, is highly disordered and dynamic, resembling an unfolded peptide tethered at one end.

Rhodopsin is the membrane-bound photoreceptor of the vertebrate rod cell and is a member of the large family of GPCR's[1] (*2*−*4*). Like all members of the family, rhodopsin is believed to contain seven transmembrane α-helices as shown in the secondary structural model of Figure 1 (*5*−*12*). Illumination of rhodopsin triggers a conformational change that apparently alters the conformation of the sequences connecting the transmembrane helices, enabling the binding and activation of G_T, the visual G protein (*13*−*17*). Shut-off of this active signaling state is initiated by phosphorylation of the rhodopsin C-terminal domain by rhodopsin kinase. Subsequent binding of arrestin to the phosphorylated domain prevents G_T activation and thereby terminates signaling (*18*, *19*). This shut-off mechanism is likely to be of general importance in other GPCR signal transduction pathways, and several related GPCR kinases and arrestins have been identified (*20*, *21*). Considering the central role of the C-terminal domain in signal shut-off (*22*), and possibly in the transport of rhodopsin (*23*, *24*), it is not surprising that mutations in this region have been linked to visual disorders (*24*, *25*). The structure and dynamics of the C-terminal domain are thus of considerable interest.

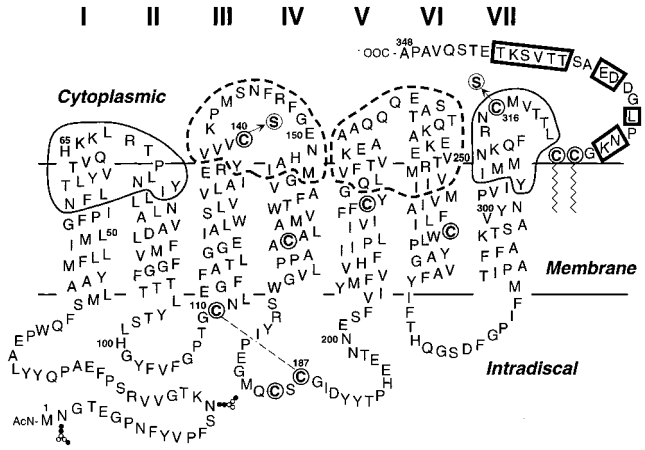

FIGURE 1: A secondary structure model of bovine rhodopsin showing the residues in the cytoplasmic domain where single-cysteine substitutions and nitroxide spin labels have been introduced. The C-terminal residues investigated in the present study are outlined with a bold rectangle. The sequences included within dashed lines were previously investigated (*5*−*8*). The sequences highlighted by a thin line are the subject of accompanying papers (*9*−*12*). In all cysteine substitution mutants, the reactive native cysteines at 140 and 316 were replaced by serine, as indicated. The secondary structures in the cytoplasmic interhelical sequences and the location of the membrane−aqueous interface relative to the helices are based on the studies referenced above.

Despite intense efforts a high-resolution structure of rhodopsin or any other member of the GPCR superfamily is not available. However, an α-carbon model for the packing of the rhodopsin helices has been constructed from electron

[†]Research reported here was supported by NIH Grants EY05216 (W.L.H.) and GM28289 (H.G.K.), the Jules Stein Professorship Endowment (W.L.H.), and a grant from the Bruce Ford Bundy and Anne Smith Bundy Foundation. R.L. is the recipient of a NRSA from the National Eye Institute.

[‡] This is paper 29 in the series "Structure and Function in Rhodopsin". The preceding paper is reference *1*.

* To whom correspondence should be addressed.

[§] University of California.

[||] Massachusetts Institute of Technology.

[1] Abbreviations: DM, dodecylmaltoside; EPR, electron paramagnetic resonance; GPCR, G-protein-coupled receptor; G_T, transducin; SDSL, site-directed spin labeling; MII, Meta II.

10.1021/bi990010g CCC: $18.00
Published on Web 05/26/1999

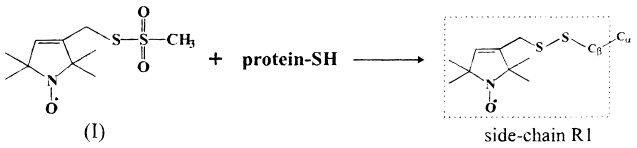

FIGURE 2: Reaction of the methanethiosulfonate derivative (I) to generate the nitroxide side chain designated R1.

density maps derived from cryoelectron microscopy (*26*, *27*). This model does not include structures for extramembranous sequences connecting the helices or the C-terminal domain, because these features are not clearly identified in the electron density maps. Solution structures for synthetic peptides corresponding to the interhelical sequences at the cytoplasmic surface and the C-terminal tail of rhodopsin have been investigated by 2D NMR (*28*−*31*), and a model for the cytoplasmic surface has been proposed (*32*).

Structural features of intact rhodopsin, including the C-terminal domain and the interhelical sequences, can be studied with SDSL. SDSL is a relatively new technique for the investigation of secondary, tertiary, and quaternary structure of both soluble and membrane-bound proteins of arbitrary molecular weight (see refs *33*−*35* for review). The strategy of SDSL requires the introduction of a nitroxide-containing side chain at selected sites in the protein. This is conveniently accomplished by cysteine substitution mutagenesis followed by modification of the unique sulfhydryl with a specific nitroxide reagent. In the studies reported below, a methanethiosulfonate reagent (I) is used to generate the nitroxide side chain designated R1 (Figure 2).

EPR analysis of R1 in a protein can provide information on the mobility and solvent accessibility of the side chain. "Mobility" is a qualitative term that describes the general dynamic state of the side chain as inferred from the CW-EPR spectral line shape. Semiquantitative measures of mobility are provided by the line width of the central ($m_I = 0$) resonance and the second moment of the spectrum (*36*). In principle, spectral simulation techniques can provide a quantitative and rigorous description of the dynamic modes of the R1 side chain (*37*, *38*). While this is not straightforward in the general case, simulation provides an effective strategy for characterizing the nearly isotropic motions encountered in regions of high backbone flexibility. This approach is taken in the present study for the estimation of the effective correlation times of R1 in the highly mobile C-terminal domain of rhodopsin. The solvent accessibility of an R1 side chain is quantitatively measured by the accessibility to collision with paramagnetic reagents, either polar or nonpolar (*33*−*35*, *39*). For a mobile side chain in a membrane protein, the hyperfine coupling constant can be used to determine whether a side chain is solvated by lipid or water (*40*).

Methods for interpreting R1 mobility and accessibility in terms of protein structure are still under development. However, it is already clear that mobility alone can provide a "fingerprint" of the tertiary fold of a protein (*36*). For example, R1 residues at buried and tertiary contact sites are strongly constrained and are relatively immobilized by the structure. On the other hand, R1 residues at exposed sites or in loop regions have relatively high mobility. In addition, sequence-specific regular secondary structure can be determined on the basis of the periodic dependence of both mobility and accessibility on sequence position (*33*, *34*). The ability to identify tertiary contact interactions and secondary structure is used in the present study to examine the fold of the rhodopsin C-terminal domain.

The SDSL method has been previously employed to examine the structure of the sequences connecting helices III and IV and helices V and VI for bovine rhodopsin in micellar solutions of DM (Figure 1). R1 scanning mutagenesis throughout these sequences identified the transmembrane helical segments and the points at which each crossed the membrane−aqueous boundary of the micelle (*6*, *8*). Moreover, a photoactivated outward tilt of the cytoplasmic part of helix VI was observed to take place coincident with the appearance of the active MII conformation (*8*, *41*). In accompanying papers, the results of systematic cysteine mutagenesis and spin labeling in the I−II interhelical sequence (*11*, *12*) and the sequence extending from helix VII to the palmitoylation sites (*9*, *10*) (Figure 1) are described.

In the present study, SDSL is used to examine the structure of the C-terminal domain of rhodopsin, extending from the palmitoylation sites at 322C and 323C to the C-terminal residue at 348. The results suggest that this domain is largely unstructured, making little or no static tertiary contacts with the remainder of rhodopsin. The backbone is dynamic throughout the sequence, with a mobility gradient pointing toward the C-terminus. The mobility in this region indicates a degree of disorder higher than that observed in any other region in rhodopsin, in contrast to the folded structure inferred from NMR studies on the isolated C-terminal peptide (*28*, *30*). The residue mobility in the 335−340 segment can be strongly modulated by binding to an antibody with an epitope at residues 341−348. However, removal of the palmitoylation sites at 322 and 323 has only a minor effect on the mobility of nearby residues 325R1 and 328R1. This latter observation indicates that the palmitoyl groups are not responsible for tethering the C-terminal domain at one end in such a way as to produce an ordered structure near 325 and 328.

EXPERIMENTAL SECTION

Preparation of the Single-Cysteine Mutants and Spin-Labeled Derivatives in the Rhodopsin C-Terminus. Single-cysteine mutants T335C, T336C, V337C, S338C, K339C, and T340C were prepared from a base mutant, in which the two reactive native cysteines C140 and C316 were replaced with serines, using fragment replacement mutagenesis as previously described (*42*). Mutant T335C was produced by the replacement of the *Bst*EII/*Nar*I restriction digest fragment (nucleotides 951−1040) in the C140S/316S construct with a synthetic oligonucleotide duplex containing the mutation at 335. Mutants T336C, V337C, S338C, K339C, and T340C were produced by replacement of the *Sal*I/*Nar*I fragment (nucleotides 999−1040) in the C140S/316S construct with synthetic oligonucleotide duplexes containing the corresponding mutation site. The codon TGC was used for cysteine.

For mutants K325C, K325C/C322S/C323S, N326C, L328C, L328C/C322S/C323S, D331C, and E332C, a two-step mutagenesis strategy was employed. PCR mutagenesis (QuickChange site-directed mutagenesis kit from Strata-

gene, La Jolla, CA) was used to generate *Pst*I and *Sal*I fragments containing the respective mutations. These fragments were subcloned into the C140S/C316S vector using the same restriction sites. The sequences of the primers were the following: 5′CTCTGCTGTGGC*TGC*AACCCGCTG3′ for K325C; 5′CTCTCTTCTGGC*TGC*AACCCGCTG3′ for K325C/C322S/C323S; 5′CTGTGGCAAG*TGC*-CCGTCGGGTG3′ for N326C; 5′GGCAAGAACCCG*T-GC*GGTGACGACG 3′ for L328C and L328C/C322S/C323S; 5′CCGCTGGGTGAC*TGC*GAGGCGTCG3′ for D331C; and 5′GGGTGACGAC*TGC*GCGTCGACCAC3′ for E332C.

All mutations were confirmed by the dideoxynucleotide sequencing method. The procedures for transient transfection of COS-1 cells with PMT4 vectors for protein expression and purification and for spin labeling were the same as those previously described (*42*). Spin-labeled mutants will be designated by giving the single-letter code for the original residue, the number of the residue, and the substituted side chain, R1, in that order. Thus S338R1 is the mutant with serine 338 replaced by the spin-labeled side chain R1.

EPR Spectroscopy. Spin-labeled rhodopsin samples (typically 5 μM in 200 μL of 5 mM MES buffer, pH 6.0, with 0.02% DM) were concentrated 10-fold using 10 kDa cutoff filters (Millipore Ultrafree). For the 1D4 antibody binding experiments, final concentrations of approximately 15 μM spin-labeled rhodopsin mutants and 25 μM 1D4 antibody, pH 7.0, were incubated for more than 10 min at room temperature prior to recording the EPR spectra. X-band EPR spectra were recorded at ambient temperature in quartz capillaries using a loop gap resonator (*43*). The scan range for all spectra is 100 G, and field modulation was selected to minimize line broadening. Final spectra were obtained by signal averaging 5−10 scans (30 s/scan). Spectra for the light-activated state were obtained after 1 min of illumination with a fiber optic illuminator (Cole Parmer, Chicago, IL) using a long-wavelength pass filter (Melles-Griot > 500 nm) and an infrared filter.

First derivative EPR spectra were normalized to the same number of spins using double integration. For two-component spectra containing a component in the fast motional regime, the individual components were obtained by subtracting a simulated fast motional spectrum from the experimental composite. The highly mobile line shape to be subtracted was computed from the theoretical stick pattern of an electron interacting with 12 equivalent protons in the α-methyl groups, 1 proton on the ring, and 6 equivalent ^{13}C nuclei at their natural abundance (1.108%). Each of the three groups of stick spectra corresponding to the ^{14}N hyperfine states was individually convoluted with a Lorentzian line of adjustable width. The simulation and subtraction were done interactively in LabVIEW (National Instruments). The adjustable parameters were the fraction of mobile component, A_N, A_H, A_C (the nitrogen, proton, and carbon hyperfine splitting constants, respectively), and the three Lorentzian line widths. Excellent fits to the mobile component were obtained with $A_N = 16.4$, $A_H = 0.21$, and $A_C = 6.90$. As a first step in the subtraction, the high-field line ($m_I = -1$) was observed and all parameters were adjusted to give the best subtraction. The criterion for the subtraction endpoint was the absence of residual sharp lines and any high-frequency oscillations in the difference spectrum. The high-field line was then fixed such that a change in A_N would not change its position. Next, A_N and the low-field ($m_I = 1$) line width were varied to optimize the subtraction at the low-field position. As a final step, the line width of the center $m_I = 0$ line was adjusted.

This procedure not only provides a resolution of the two spectral components but also provides homogeneous Lorentzian line widths for the hyperfine components of the highly mobile component. For R1 residues in the fast motional regime ($\tau \leq 1 \times 10^{-9}$ s), these line widths were used to compute the rotational correlation times according to the approximate model of Stone et al. (*44*). The correlation times computed from the linear and quadratic terms in m_I were within a factor of 2 of each other, and the motion is effectively isotropic. The value reported below is the geometric mean of the two.

For slower R1 motions with a correlation time longer than 1×10^{-9} s, the effective correlation time was estimated by spectral simulation (*37*, *38*). In the simulations, the experimental spectra were fit in a least-squares sense with the principle components of the rotational diffusion (**R**), hyperfine (**A**), and g (**g**) tensors, and the Gaussian inhomogeneous line width as parameters. In the case of **A** and **g**, the values were allowed to vary only over a narrow range corresponding to known values in water solution. The effective correlation time for the best fit is computed as $\tau = 1/6R^*$, where $R^* = (R_{xx}R_{yy}R_{zz})^{1/3}$ (*37*).

RESULTS

Mobility at Selected Sites in the C-Terminal Domain of Rhodopsin. The single-cysteine mutants were all prepared from a "base" mutant in which the reactive native cysteines C140 and C316 were replaced with serine. However, the native cysteines C110, C167, C185, C187, C222, and C264, and those at the palmitoylation sites C322 and C323 were retained. Cysteines 110 and 187 form a disulfide bond and are unreactive. Likewise, cysteines 322 and 323 are palmitoylated and unreactive. Spin labeling of this base mutant gives a weak EPR signal due to limited reaction of (I) with the remaining cysteines (Figure 3, top). As shown in a previous characterization of this base mutant, the background signal corresponds to less than 0.3 spins/rho (*45*).

To investigate the secondary structure and the dynamics of the C-terminal domain in rhodopsin, we replaced the native residues at 325, 326, 328, 331, 332, and 335−340 in the base mutant one at a time with cysteine. Each of the mutants reacted with the methanethiosulfonate reagent (I) in the dark to give the EPR spectra shown in Figure 3 (solid line). It is apparent that the spectrum of the base mutant makes only a small contribution to the intensity and shape of the spectra in Figure 3.

A striking feature of these normalized spectra is the regular amplitude increase from 325R1 to 340R1. The amplitude increase is a result of a decrease in spectral line width, which is in turn due to an increase in R1 mobility. Thus, there is an effective gradient in mobility along the C-terminal domain, with the most mobile sites being farthest from the palmitoylation sites. For convenience, the labeled sites will be divided into the following three groups: 325R1−328R1, the residues closest to the palmitoylation sites; 331R1 and 332R1, residues at an intermediate position; and 335R1−

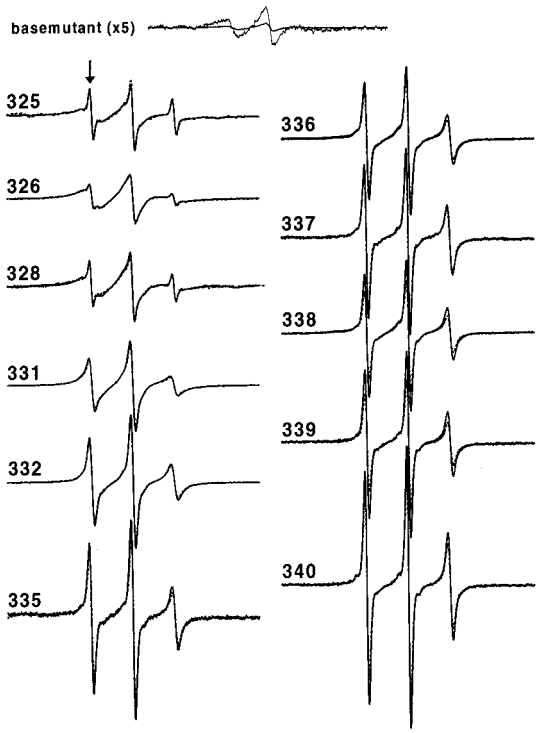

FIGURE 3: EPR spectra of R1 side chains at the indicated positions in the C-terminal domain in the dark (solid line) and photoactivated (dashed line) state. The spectra are normalized to the same number of spins. The EPR spectrum of the base mutant is shown in the inset at the top of the figure. This spectrum is approximately normalized to the same amount of protein used to obtain the spectra for the mutants. The arrow highlights the location of the highly mobile component in one of the three spectral lines for the 325R1 derivative.

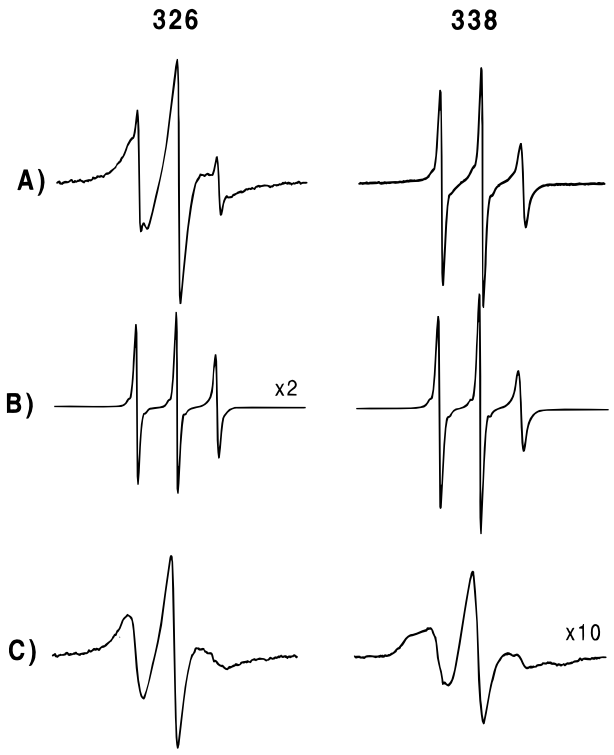

FIGURE 4: Analysis of the EPR spectra of 326R1 and 338R1 in terms of two components. (A) The experimental composite spectrum; (B) the mobile component (simulated); (C), the difference spectrum (A − B). The dotted trace in part C is the simulated spectrum. The salient parameters were the following: A_{xx}= 6.3 G, A_{yy} = 5.57 G, A_{zz}= 36.08 G, G_{xx} = 2.0088, G_{yy} = 2.0064, G_{zz} = 2.00237, R_{xx} = 7.9 × 10^6/s, R_{yy} = 1.1 × 10^8/s, and R_{zz} = 1.1 × 10^8/s. The relative amount of mobile component is 3% for 326R1 and 50% for 338R1.

340R1, the residues near the end of the domain, adjacent to the epitope of the 1D4 antibody (residues 341−348) used in rhodopsin purification. Within each group, the EPR spectra have similar characteristics.

The EPR spectra in Figure 3 have two components. This is readily apparent in the group 325R1−328R1 where a minor sharp component (arrow) is resolved from a broader component reflecting a less mobile spin population. Although it is not as obvious, the other spectra also have two components. In all cases, one component has sharp resonance lines corresponding to rapid and effectively isotropic motion. Under these conditions, the two components can be resolved by the simulation−subtraction procedure described in the Experimental Section. As examples, the individual spectral components for 326R1 and 338R1, representing the groups at the beginning and end of the C-terminal sequence, are shown in Figure 4. For 326R1, the component corresponding to high mobility is minor, representing only about 5% of the total population (Figure 4B), while the dominant component is of intermediate mobility (Figure 4C). The effective correlation time corresponding to this latter spectrum is about 3.5 ns, as determined by simulation (Figure 4C, dotted line).

For 338R1, a highly mobile component is the dominant state, representing 65−70% of the total population (Figure 4B), with a second population of lower mobility (Figure 4C). The EPR spectra of other sites in the group 335R1−340R1 are similar to that of 338R1, and an analysis shows that the highly mobile component varies from 80% to nearly 100% of the population. Thus, these sites are best characterized by a dominant population of unusually high mobility. The effective correlation time for R1 at these sites is in the range 0.3−0.5 ns, similar to that for R1 in unfolded proteins (*35*, *46*, *47*). The EPR spectra of the minor populations are all similar to that shown in Figure 4C for 338R1 (data not shown).

The spectra of the intermediate group 331R1 and 332R2 could not be simulated using a single spin population. Simulations using two components gave fits of quality similar to that shown for 326R1 (Figure 4C). The dominant (80−90%) and minor populations have correlation times of about 2 and 0.4 ns, respectively.

In summary, all of the sites apparently have multiple populations of different mobility, but in each case, one is clearly dominant. For the dominant populations, there is a clear gradient of mobility along the C-terminal domain. The effective correlation times decrease from ≈3.5 ns at sites adjacent to the palmitoylation residues (325R1−328R1) to ≈2 ns at the intermediate sites 331R1 and 332R1 to 0.3−0.5 ns near the end of the domain (335R1−340R1). A mobility gradient of this type is expected for a free polypeptide chain tethered at one end. The nitroxides in the dominant states are all water-exposed, judging from the apparent hyperfine coupling of 16.5 G (*40*).

Consequences of 1D4 Antibody Binding to the C-Terminal Domain. To explore the validity of the tethered chain model for the C-terminal domain, we investigated the effect of 1D4 antibody binding on the mobility of 335R1 to 340R1. The

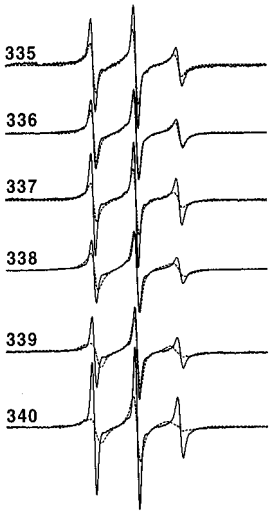

FIGURE 5: Effect of 1D4 antibody binding on the mobility of R1 side chains in the C-terminal domain (335−340). The solid and dashed lines are the spectra in the absence and presence of the antibody, respectively.

1D4 antibody recognizes an epitope at residues 341−348 at the end of the C-terminal domain and is an important reagent for the purification of rhodopsin (*48*). Figure 5 shows the effect of the binding of 1D4 antibody on the EPR spectra of 335R1−340R1, the sites closest to the epitope. Antibody binding causes simple line broadening with a concomitant decrease in signal amplitude indicative of a decrease in mobility. This effect is most pronounced for the residues 339R1 and 340R1, closest to the epitope, and weakest at 335R1 and 336R1, furthest from the epitope. Thus, antibody binding induces a gradient in mobility along the polypeptide consistent with the introduction of a new tether point at the extreme C-terminus. In the presence of bound antibody, the C-terminal domain resembles a flexible chain anchored at both ends (a "jump-rope"). Even in the presence of bound antibody, however, the R1 spectra reflect a dynamic state. For example, the effective correlation time for 340R1 with bound antibody is ≈3 ns, compared to ≈0.5 ns in the absence of antibody.

Effect of Palmitoylation. The data presented so far were obtained from rhodopsin mutants with the palmitoylation sites intact. To assess the role of palmitoylation in the formation of the mobility gradient in the C-terminal domain, we recorded spectra of R1 at selected C-terminal residues in the absence of palmitoylation. The nonpalmitoylated derivatives were obtained using the base mutant with the additional substitutions C322S and C323S. Because any effect should be largest near the palmitoylation sites, 325R1 and 328R1 were selected for study. To examine effects distant from the palmitoylation sites, we selected 338R1 as a representative.

The EPR spectra for 325R1, 328R1, and 338R1 in the presence and absence of palmitoylation are compared in Figure 6. Surprisingly, the effect of removing the palmitoylation sites is small and highly localized. The spectra of proximal sites 325R1 and 328R1 retain their essential two-component character, with apparently only minor increases in the relative population of the more mobile state. The spectral properties of 338R1 are virtually unchanged. Thus, the palmitoyl chains at 322 and 323 in native rhodopsin in DM solutions seem to play a minor role in anchoring one end of the C-terminal domain.

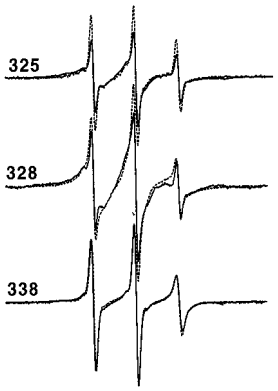

FIGURE 6: Effect of palmitoylation on the mobility of R1 side chains at 325, 328, and 338. For each site, the solid trace is the spectrum of the spin-labeled mutant with wild-type palmitoylation, and the dashed trace is the spectrum in the absence of palmitoylation.

Light-Dependent Changes. The spectra of R1 at sites in the C-terminal domain exhibit a small but detectable light-dependent change that results in the loss of signal amplitude at many sites, most notably those in the 335R1−340R1 group (see dashed lines, Figure 3). This loss in signal amplitude is due to a slight increase in the less mobile population at the expense of the more mobile one. However the effect is small and the data suggest that the highly dynamic and unstructured state of the C-terminal domain is similar in the dark- and light-activated forms. In the presence of bound 1D4 antibody, no light-dependent changes could be detected.

DISCUSSION

The C-terminal domain of rhodopsin is defined as the sequence extending from the palmitoylation sites at C322 and C323 to the C-terminus. The primary conclusion to be drawn from the results presented above is that the dominant state of the C-terminal domain is best characterized as an unfolded polypeptide chain tethered at one end. The evidence for this conclusion is of three kinds. First, the average residue mobility is high throughout the full length of the polypeptide (Figure 3). In fact, the effective correlation time for R1 residues in the group 335R1−340R1 near the end of the domain (correlation time ≈ 0.3−0.5 ns) is comparable to that observed in small peptides and unfolded proteins (*35*, *46*, *47*, *49*, *50*). For reference, the correlation time of a small nitroxide free in solution is ≈0.03 ns. The 325R1−328R1 residues adjacent to the palmitoylation sites have the lowest mobility in the C-terminal domain, yet they have mobility similar to that in dynamic loops in soluble proteins (*36*). Second, a mobility gradient exists along the C-terminal domain, with increasing mobility toward the C-terminus as reflected in the spectral intensity increase from 325R1 to 340 R1 (Figure 3). Such a gradient is expected for a free polypeptide chain tethered at one end, similar to the situation for hydrocarbon chains in a bilayer tethered at the headgroup region (*51*). Finally, the effect of the 1D4 antibody binding is consistent with the above model. Binding of 1D4 would be predicted to provide a second tether point at the C-terminus. Thus, in the presence of the antibody the C-terminal domain would be tethered at both ends, with mobility gradients pointing toward the center from either tether point.

These effects are in fact observed experimentally (Figures 3, 5).

Surprisingly, removal of the palmitoylation sites in the base mutant by the substitutions C322S/C323S had little effect on the mobility gradient (Figure 6). This demonstrates that the palmitoyl groups are not an integral part of the structural tether on the N-terminal part of the sequence. In accompanying papers, it is shown that the sequence 316−321, leading up to the palmitoylation sites from the N-terminal side, is in strong tertiary interaction with the rest of the protein (*9*, *10*). Thus, this region likely constitutes the tether.

The spectra of R1 in the C-terminal domain have two components corresponding to spin populations of different mobility. For the 325R1−328R1 group, the minor component is of little consequence, being only about 5% of the population. For the 335R1−340R1 group, the minor component is of intermediate mobility, and can comprise as much as 30−35% of the spectrum, although it is typically less. The origin and significance of this minor component are unknown, but there are two likely possibilities. First, part of this signal undoubtedly comes from the background of native sulfhydryls in the rhodopsin base mutant (Figure 3, top). However, light activation appears to cause a small interconversion of the populations, suggesting a light-dependent equilibrium between the two components. This would be difficult to explain if all of the minor components were due to background signal. In addition, the amount of the minor component varies significantly from site to site, whereas the amount of background would be constant. Another possible origin of the minor population is simply adsorption of the flexible C-terminal peptide on the micelle surface. This would not be surprising, and such an adsorption may be enhanced at select positions by the presence of the relatively hydrophobic R1 side chain.

In a recent study it was found that the rhodopsin phosphorylation site S338 was in close proximity to the cytoplasmic extension of helix VI (*42*). Other phosphorylation sites are found in the region from residue 334 through residue 343. According to the spectra of all of the residues we investigated in this sequence (residues 335−340), this region is highly disordered and likely to have a random coil geometry. This region must then extend into the aqueous environment but remain localized near the solvent-exposed face of the cytoplasmic portion of helix VI. However, the high mobility of sites in the C-terminal domain argues against a stable interaction with helix VI.

Yeagle and co-workers recently determined the structure of a peptide corresponding to the C-terminal domain of rhodopsin using 2D NMR methods (*28*, *30*). The peptide was found to have an antiparallel β-sheet conformation for the region containing the phosphorylation sites, with residues 335 and 337 at buried sites in the structure and residues 336 and 338 at solvent-exposed surface sites. This is at odds with the high mobility seen in the EPR spectra for R1 throughout this region. In particular, 335R1 and 337R1 are among the most mobile residues, with no evidence of tertiary contact interactions that would result in immobilization. It is possible that substitution of R1 at buried sites such as 335 and 337 could cause destabilization and unfolding of a small domain, giving rise to the high mobility of R1 at such sites. Indeed, it has been found that R1 at buried sites in T4 lysozyme can cause destabilization of up to 4 kcal/mol, similar to substitutions for alanine at the same sites (*36*). For T4 lysozyme, this destabilization is not sufficient to significantly change the structure at room temperature, but for a small domain it could be enough to cause unfolding. On the other hand, there is abundant evidence that R1 substituted at solvent-exposed surface sites causes little or no destabilization and sometimes stabilization (*36*). If the C-terminal domain of rhodopsin had a stable tertiary structure, R1 at surface sites should have partial immobilization due to the constrained backbone dynamics and possible interactions with neighboring side chains (*35*). However, as shown above, the variation in mobility of R1 side chains is described as a simple gradient along the C-terminal domain rather than the site-specific variation expected of a folded protein. Therefore, it seems unlikely that the C-terminal domain has a stable folded structure.

The primary interaction sites of rhodopsin and rhodopsin kinase have been mapped to the cytoplasmic interhelical sequences on rhodopsin rather than the C-terminal domain that contains the substrate for phosphorylation (*52*, *53*). In fact, rhodopsin kinase interacts with a C-terminal truncation mutant in a light-dependent fashion (*54*). Thus, the light-activated binding of the kinase is not due to exposure of the C-terminal substrate, but must be triggered by changes in other parts of the molecule. This is consistent with the exposed, dynamic state of the C-terminal domain, independent of photoactivation (*21*) (Figure 3). Moreover, a loose and dynamic structure of the C-terminus is in accord with its role as substrate for rhodopsin kinase. It has been shown that many of the C-terminal Ser and Thr residues can be phosphorylated by rhodopsin kinase. A well-packed structure in the C-terminal domain would work against rapid phosphorylation of these sites, because an unfolded state would likely be required to accommodate all of these residues into the active site.

ACKNOWLEDGMENT

We thank David Budil, Northeastern University, for providing us with the spectral simulation program.

REFERENCES

1. Eilers, M., Reeves, P. J., Ying, W., Khorana, H. G., and Smith, S. O. (1999) *Proc. Natl. Acad. Sci. U.S.A. 96*, 487−492.
2. Helmreich, E. J. M., and Hofman, K. P. (1996) *Biochim. Biophys. Acta 1286*, 285−322.
3. Wess, J. (1997) *FASEB J. 11*, 346−354.
4. Sakmar, T. P. (1998) *Prog. Nucleic Acid Res. Mol. Biol. 59*, 1−34.
5. Ridge, K. D., Zhang, C., and Khorana, H. G. (1995) *Biochemistry 34*, 8804−8811.
6. Farahbakhsh, Z. T., Ridge, K. D., Khorana, H. G., and Hubbell, W. L. (1995) *Biochemistry 34*, 8812−8819.
7. Yang, K., Farrens, D. L., Hubbell, W. L., and Khorana, H. G. (1996) *Biochemistry 35*, 12464−12469.
8. Altenbach, C., Yang, K., Farrens, D. L., Farahbakhsh, Z. T., Khorana, H. G., and Hubbell, W. L. (1996) *Biochemistry 35*, 12470−12478.
9. Cai, K., Klein-Seetharaman, J., Farrens, D., Zhang, C., Altenbach, C., Hubbell, W. L., and Khorana, H. G. (1999) *Biochemistry 38*, 7925−7930.
10. Altenbach, C., Cai, K., Khorana, H. G., and Hubbell, W. L. (1999) *Biochemistry 38*, 7931−7937.
11. Klein-Seetharaman, J., Hwa, J., Cai, K., Altenbach, C., Hubbell, W. L., and Khorana, H. G. (1999) *Biochemistry 38*, 7938−7944.

12. Altenbach, C., Klein-Seetharaman, J., Khorana, H. G., and Hubbell, W. L. (1999) *Biochemistry 38*, 7945−7949.
13. Kuhn, H., and Hargrave, P. A. (1981) *Biochemistry 20*, 2410−2417.
14. Konig, B., Arendt, A., McDowell, J. H., Kahlert, M., Hargrave, P. A., and Hofmann, K. P. (1989) *Proc. Natl. Acad. Sci. U.S.A. 86*, 6878−6882.
15. Franke, R. R., Konig, B., Sakmar, T. P., Khorana, H. G., and Hofman, K. P. (1990) *Science 250*, 123−125.
16. Franke, R. R., Sakmar, T. P., Graham, R., and Khorana, H. G. (1992) *J. Biol. Chem. 267*, 14767−14774.
17. Ernst, O. P., Hofmann, K. P., and Sakmar, T. P. (1995) *J. Biol. Chem. 270*, 10580−10586.
18. Miller, J. L., Fox, D. A., and Litman, B. J. (1986) *Biochemistry 25*, 4983−4988.
19. Wilden, U., Hall, S. W., and Kühn, H. (1986) *Proc. Natl. Acad. Sci. U.S.A. 83*, 1174−1178.
20. Lefkowitz, R. J. (1993) *Cell 74*, 409−412.
21. Palczewski, K. (1997) *Eur. J. Biochem. 248*, 261−269.
22. Chen, J., Makino, C. L., Peachey, N. S., Baylor, D. A., and Simon, M. I. (1995) *Science 267*, 374−377.
23. Sung, C. H., Makino, C., Baylor, D., and Nathans, J. (1994) *J. Neurosci. 14*, 5818−5833.
24. Li, T., W. K., S., Olsson, J. E., and Dryja, T. P. (1996) *Proc. Natl. Acad. Sci. U.S.A. 93*, 14176−14181.
25. Nathans, J. (1994) *Cell 78*, 357−360.
26. Baldwin, J., Schertler, G. F. X., and Unger, V. M. (1997) *J. Mol. Biol. 272*, 144−164.
27. Unger, V. M., Hargrave, P. A., Baldwin, J. M., and Schertler, G. F. X. (1997) *Nature 389*, 203−206.
28. Yeagle, P. L., Alderfer, J. L., and Albert, A. D. (1995) *Nat. Struct. Biol. 2*, 832−834.
29. Yeagle, P. L., Alderfer, J. L., and Albert, A. D. (1995) *Biochemistry 34*, 14621−14625.
30. Yeagle, P. L., Alderfer, J. L., and Albert, A. D. (1996) *Mol. Vis. 2*, 12.
31. Yeagle, P. L., Alderfer, J. L., and Albert, A. D. (1997) *Biochemistry 36*, 3864−3869.
32. Yeagle, P. L., Alderfer, J. L., and Albert, A. D. (1997) *Biochemistry 36*, 9649−9654.
33. Hubbell, W. L., Gross, A., Langen, R., and Lietzow, M. A. (1998) *Curr. Opin. Struct. Biol. 8*, 649−656.
34. Hubbell, W. L., and Altenbach, C. (1994) *Curr. Opin. Struct. Biol. 4*, 566−573.
35. Hubbell, W. L., Mchaourab, H. S., Altenbach, C., and Lietzow, M. A. (1996) *Structure 4*, 779−783.
36. Mchaourab, H. S., Lietzow, M. A., Hideg, K., and Hubbell, W. L. (1996) *Biochemistry 35*, 810−822.
37. Budil, D. E., Lee, S., Saxena, S., and Freed, J. H. (1996) *J. Magn. Reson. 120*, 155−189.
38. Freed, J. H. (1976) *Spin Labeling: Theory and Applications* (Berliner, L. J., Ed.) Vol. 1, Academic Press, New York
39. Altenbach, C., Flitch, S., Khorana, H. G., and Hubbell, W. L. (1989) *Biochemistry 28*, 7806−7812.
40. Griffith, O. H., and Jost, P. C. (1976) *Spin Labeling: Theory and Applications* (Berliner, L. J., Ed.) Vol. 1, Academic Press, New York.
41. Farrens, D. L., Altenbach, C., Yang, K., Hubbell, W. L., and Khorana, H. G. (1996) *Science 274*, 768−770.
42. Cai, K., Langen, R., Hubbell, W. L., and Khorana, H. G. (1997) *Proc. Natl. Acad. Sci. U.S.A. 94*, 14267−14272.
43. Hubbell, W. L., Froncisz, W., and Hyde, J. S. (1987) *Rev. Sci. Instrum. 58*, 1879−1886.
44. Stone, T. J., Buckman, T., Nordido, P. L., and McConnell, H. M. (1965) *Proc. Natl. Acad. Sci. U.S.A. 54*, 1010−1017.
45. Resek, J. F., Farahbakhsh, Z. T., Hubbell, W. L., and Khorana, H. G. (1993) *Biochemistry 32*, 12025−12031.
46. Klug, C. S., and Feix, J. B. (1998) *Protein Sci. 7*, 1469−1476.
47. Qu, K. B., Vaughn, J. L., Sienkiewicz, A., Scholes, C. P., and Fetrow, J. S. (1997) *Biochemistry 36*, 2884−2897.
48. Oprian, D. D., Molday, R. S., Kaufman, R. J., and Khorana, H. G. (1987) *Proc. Natl. Acad. Sci. U.S.A. 84*, 8874−8878.
49. Miick, S. M., Martinez, G., Fiori, W. R., Todd, A. P., and Millhauser, G. L. (1992) *Nature 359*, 653−655.
50. Qin, Z. H., Wertz, S. L., Jacob, J., Savino, Y., and Cafiso, D. S. (1996) *Biochemistry 35*, 13272−13276.
51. Hubbell, W. L., and McConnell, H. M. (1971) *J. Am. Chem. Soc 93*, 314−326.
52. Shi, W., Osawa, S., Dickerson, C. D., and Weiss, E. R. (1995) *J. Biol. Chem. 270*, 2112−2119.
53. Thurmond, R. L., Creuzenet, C., Reeves, P. J., and Khorana, H. G. (1996) *Proc. Natl. Acad. Sci. U.S.A. 94*, 1715−1720.
54. Palczewski, K., Buczylko, J., Kaplan, M. W., Polans, A. S., and Crabb, J. W. (1991) *J. Biol. Chem. 266*, 12949−12955.

BI990010G